Phenotypic model for early T-cell activation displaying sensitivity, specificity, and antagonism

Paul François[a,1], Guillaume Voisinne[b], Eric D. Siggia[c,1], Grégoire Altan-Bonnet[b], and Massimo Vergassola[c,d,e]

[a]McGill University, Montreal, QC, Canada H3A 2T8; [b]ImmunoDynamics Group, Programs in Computational Biology and Immunology, Memorial Sloan–Kettering Cancer Center, New York, NY 10065; [c]The Rockefeller University, New York, NY 10065; [d]Institut Pasteur, 75724 Paris Cedex 15, France; and [e]Centre National de la Recherche Scientifique, Unité Mixte de Recherche 3525, F-75015 Paris, France

Contributed by Eric D. Siggia, January 16, 2013 (sent for review October 29, 2012)

Early T-cell activation is selected by evolution to discriminate a few foreign peptides rapidly from a vast excess of self-peptides, and it is unclear in quantitative terms how this is possible. We show that a generic proofreading cascade supplemented by a single negative feedback mediated by the Src homology 2 domain phosphatase-1 (SHP-1) accounts quantitatively for early T-cell activation, including the effects of antagonists. Modulation of the negative feedback with SHP-1 concentration explains counterintuitive experimental observations, such as the nonmonotonic behavior of receptor activity on agonist concentration, the digital vs. continuous behavior on certain parameters, and the loss of response for high SHP-1 concentration. New experiments validate predictions on the nontrivial joint dependence on binding time and concentration for the relative effect of two antagonists: We explain why strong antagonists behave as partial agonists at low concentration and predict that the relative effect of antagonists can invert as their concentrations are varied. By focusing on the phenotype, our model quantitatively fits a body of experimental data with minimal variables and parameters.

kinetic proofreading | modeling | systems immunology | immune system

In vertebrates, T lymphocytes constantly scan the surface of antigen-presenting cells (APCs) for the detection of foreign peptide fragments bound in the peptide-MHC (pMHC). Recognition takes place via the pMHC binding to T-cell receptors (TCRs) and the transduction of the signal via the downstream signaling cascade. It is essential that T cells be activated when binding to foreign peptides occurs and not when confronted with self-peptides. Failures in the discrimination process result in either infection or autoimmune diseases (1).

The T-cell signal transduction system is experimentally found to satisfy a tight set of properties, all necessary for appropriate initiation of the immune response (1):

Speed: TCRs have to scan a large number of APCs to detect the rare foreign peptide; thus, discrimination speed is essential. Experiments provide direct visualizations of the treadmill-like process of scanning (2–4) and indicate that interactions last in the range of 1–5 min. Discrimination among antigens is achieved within this time window. The binding between the pMHC and activated T cells is subsequently stabilized and restructured by dynamical processes, such as the formation of the immunological synapse (5).

Sensitivity: T cells recognize foreign ligands even in minute amounts (6, 7); that is, 10 agonist ligands charged on APCs activate lymphocytes and the immune response.

Specificity: On the contrary, T cells usually do not respond to self-ligands, even if presented in numbers as high as 10^5 or more.

Any model of early T-cell response must be compatible with these three properties.

A natural and elegant early hypothesis proposed that antigen discrimination would be achieved mostly through structural rearrangements specific to agonists (8). However, experimental data have not identified strong causal relations between structural modifications of the receptors and the type of antigen bound. Existing experimental evidence points rather to the lifetime τ of the TCR–pMHC complex as the major determinant in the discrimination process (9). Self-ligands typically have a short lifetime (i.e., dissociate rapidly), whereas foreign ligands stay bound to TCRs for longer typical times. It should be pointed out, however, that some ligands with very strong binding constants and shorter lifetime can also trigger responses. One explanation is that they reassociate after unbinding so quickly that their effective binding time is much longer (10, 11).

An idealized immune response in terms of ligand concentration vs. dissociation time is summarized in Fig. 1*A*. There is some debate on the precise value of dissociation times in vivo compared with experiments in solution (12, 13). Experiments with cells isolated from ovalbumin-specific TCR transgenic line 1 (OT-1) mice present a "threshold" for activation around $\tau = 3$–5 s, and a three- to fivefold increase in τ is sufficient to distinguish antigens that activate T cells (agonists) from those that do not (nonagonists) (14).

The few-fold difference in affinity between agonists and nonagonists is insufficient to compensate for their orders-of-magnitude difference in potency as long as only equilibrium thermodynamic processes are considered. However, out-of-equilibrium kinetic proofreading (KPR) provides a mechanism that amplifies differences in affinity and could permit discrimination (15, 16). This possibility was originally recognized and proposed for immunology by McKeithan (17). Phosphorylation processes postulated in the KPR scheme are indeed compatible with the existing molecular evidence of immunoreceptor tyrosine-based activation motif (ITAM) sites on the cytoplasmic side of TCRs (1). However, KPR amplification of discrimination requires a sufficiently large number of phosphorylation layers and a strong bias toward

Significance

Early immune response has to discriminate a few foreign peptides rapidly from a vast excess of self-peptides, and it is unclear in quantitative terms how this is possible. We show that a generic proofreading cascade supplemented by a single negative feedback mediated by the Src homology 2 domain phosphatase-1 (SHP-1) accounts quantitatively for this discrimination. Our model, with minimal variables and parameters, can fit a large body of experimental data and accounts for phenotypes in T-cell activation. New experiments validate our predictions and provide a quantitative understanding of antagonism, the effect by which foreign ligands close to activation alter the immune response.

Author contributions: P.F., G.V., E.D.S., G.A.-B., and M.V. designed research, performed research, contributed new reagents/analytic tools, analyzed data, and wrote the paper.

The authors declare no conflict of interest.

[1]To whom correspondence may be addressed. E-mail: paulf@physics.mcgill.ca or siggiae@rockefeller.edu.

This article contains supporting information online at www.pnas.org/lookup/suppl/doi:10.1073/pnas.1300752110/-/DCSupplemental.

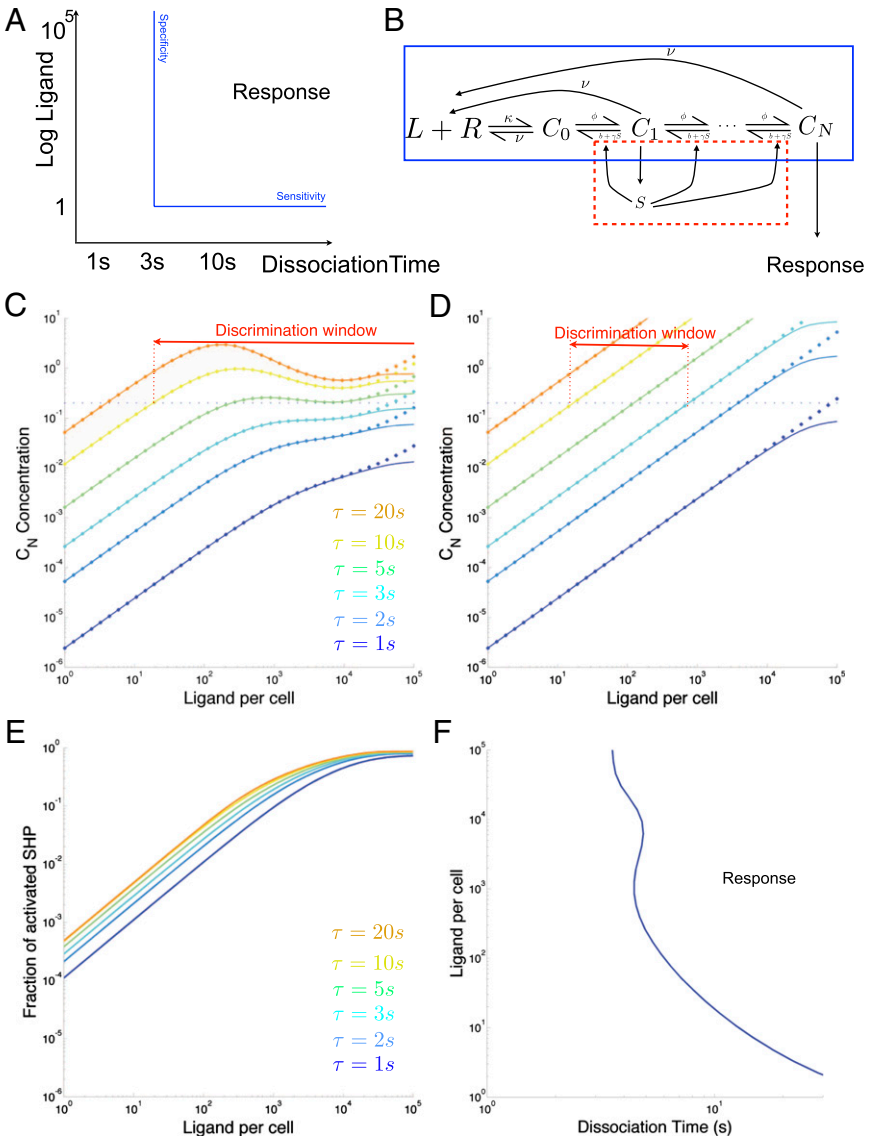

Fig. 1. Scheme of our model for early T-cell response and its behavior. (*A*) Idealized sensitivity-specificity curve of the immune response as a function of ligand concentration and dissociation time. Antigen discrimination is supposed to hinge on the antigen-TCR dissociation time. (*B*) Our model of KPR with negative feedback. The blue box indicates the core KPR, and the red box illustrates the negative feedback mediated by phosphatase, assumed to be SHP-1. Equations are defined in *SI Appendix*. (*C*) Numerical integration for the steady-state concentration of the effector C_N, which controls the response of the system, as a function of antigen concentration for different dissociation times. All concentrations are expressed per cell. Parameters used are as in Table 1. Threshold K on C_N for activation of response is indicated by the dotted line. The color (from blue to orange) corresponds to values of τ =1, 2, 3, 5, 10, and 20 s. Crosses indicate the analytical derivation performed in *SI Appendix* assuming no receptor saturation. The discrimination range in antigen concentration between τ = 3 s and τ =10 s is indicated by the red arrow. (*D*) Numerical integration of the system of equations with no phosphatase (i.e., pure KPR) for comparison. The discrimination range in antigen concentration between 3 and 10 s is indicated by the red arrow. Crosses indicate analytical KPR without receptor saturation. (*E*) Fraction of activated SHP-1 as a function of antigen concentration for different dissociation times (same color code as in *C* and *D*). SHP-1 controls the strength of the negative feedback; it increases with ligand number but clearly does not depend much on the dissociation time. (*F*) Concentration of antigen-triggering response as a function of its dissociation time. Note that for intermediate dissociation time, the response can disappear for a small range of high ligand concentrations. From this curve, one can define the agonist region for $\tau > 3$ s; the response is specific. For 3 s $< \tau <$ 10 s, ligand concentration to trigger response drops from more than 100,000 to values of order 10, spanning ligand concentrations across four orders of magnitude; the response is sensitive.

the dissociation of the TCR–pMHC complex. These features are incompatible (see below) with the observed fast response times (only roughly 10-fold longer than typical lifetimes of the TCR–pMHC complex) and the small number of antigens required for activation that we mentioned above. Furthermore, the linearity of KPR cannot account for the observed phenomenon of antagonism, whereby the presence of nonagonists can inhibit the response to agonists (18).

Germain and colleagues (19) added to the basic KPR process a negative feedback mediated by Src homology 2 domain phosphatase-1 (SHP-1) and a positive feedback mediated by ERK kinase. Their insights were codified in a very elaborate model that, given plausible parameters, was able to satisfy the constraints of speed, sensitivity, and specificity (14, 20). Subsequent experimental work, informed by the model, identified parameters (i.e., concentrations of key effectors, such as SHP-1 and CD8) that can quantitatively tune the immune response in either a digital or analog way (21). Another model (22) was built on the premise that when the agonist concentration is very low, the foreign peptides must cooperate with endogenous peptides to

activate T cells (23). To satisfy the speed, sensitivity, and selectivity constraints, they required additional feedback onto the relevant KPR kinase, lymphocyte-specific protein tyrosine kinase (Lck). This model was also quite elaborate, with upward of 50 parameters, and had to be solved stochastically to explain experiments.

Here, we propose a phenotypic model for early T-cell activation that relies on just the SHP-1 feedback and can be largely solved analytically. It has just nine relevant parameters (with only seven for the steady state). The model does not require any cooperativity between self and foreign peptides at low agonist levels, which could, however, contribute supplementary modulation as suggested by Yachi et al. (24) and Ma et al. (25). Our model recapitulates all the data used to validate the prior model (14), as well as the observations by Feinerman et al. (21), as to speed/sensitivity/specificity and the digital/analog responses with variation of key effector concentrations. The stochastic version of our model rounds transitions in the deterministic model but is otherwise very similar.

Our model accounts for previously unexplained observations. In particular, we reanalyze the counterintuitive collapse of the response at high ligand concentrations for weak agonists and tie it to the activity of the phosphatase SHP-1 (14). We further show and explain why increasing the SHP-1 concentration also results in the loss of response at high agonist concentrations (21). Finally, we use our model mathematically to characterize antagonistic effects, identifying a tradeoff for antagonism between antagonist lifetime and concentration. These predictions are experimentally tested and verified.

We model the phenotype rather than every protein and phosphorylation state, and thereby obtained a model simple enough to solve algebraically yet able to fit all available data with each parameter plausibly linked to one or a few molecular components. Simplified models are sometimes more predictive than elaborate ones when data are sparse and have the added benefit of transparency.

Results

Model Based on KPR with Feedback. The KPR scheme proposed by McKeithan (17) assumes a cascade of phosphorylations of the antigen–receptor complex, with the level of the last component of the cascade controlling the response and activation (Fig. 1*B*, blue box with the definition of parameters).The sequence of phosphorylated complexes C_i can be biologically interpreted as surrogates for the numerous ITAM phosphorylations (2, 26) by kinase Lck (recruited by coreceptor CD8). We assume a forward phosphorylation rate ϕ and a default dephosphorylation rate b. On ligand unbinding (rate $\upsilon = 1/\tau$), the complex is assumed to be instantaneously dephosphorylated into unoccupied receptor [if dephosphorylation is not instantaneous, fast binders would reassociate before dephosphorylation of the whole cascade, which could explain the longer effective binding times observed by Govern et al. (10) and Aleksic et al. (11)]. We assume that constitutive phosphatases (e.g., CD45) control these dephosphorylations.

The analytical calculation of the steady-state concentration for the KPR model is recalled in *SI Appendix*. In the limit of unsaturated receptors and strong dissociation rate of the antigen–receptor complex, one finds that the last layer of the cascade $C_N \propto Lr(\upsilon,\phi,b)^N$, where $r(\upsilon,\phi,b)$, is the solution of the characteristic Eq. **S15** in *SI Appendix* (see also Eq. **S28**) and L is the number of antigenic ligands. The geometric exponent N corresponds to the number of phosphorylation steps in the cascade: The more steps there are, the more sensitive $r(\upsilon,\phi,b)^N$ is to differences in dissociation times among ligands, which can then be used for their discrimination. However, as already mentioned in the introductory section, KPR alone is insufficient to capture all the dynamical properties of the ligand discrimination system. Indeed, as discussed by Altan-Bonnet and Germain (14), the value of N necessary to achieve the observed discrimination among antigens is relatively large. This would lead to large ratios between the activation time and τ, as well as to the fact that many agonists L would be required to have the final effector C_N of order unity. Rapidity and sensitivity of response would thus be lost at the expense of specificity. Finally, the response of KPR far from receptor saturation is linear in ligand concentration, which is not compatible with the experimental observation of antagonistic effects (18) and dose–response curves (protocol S1 in ref. 14).

To capture the dynamics of T-cell signaling and still retain a simple model, we add a single component (Fig. 1*B*, red box) accounting for the effect of negative feedback on proofreading. This feedback could have multiple molecular origins in the real network. Following Altan-Bonnet and Germain (14), SHP-1 provides one example of a phosphatase that has the properties required for the feedback discussed in our model. In the interest of concreteness, we shall henceforth refer in the sequel to SHP-1 as the main effector, even though the molecular implementation of the feedback might actually be more elaborate. We further assume that concentration of SHP-1 is fixed on the T-cell early response time scales and that the first phosphorylated complex C_1 in the cascade phosphorylates SHP-1 and activates it. Similar behaviors are obtained when activation comes from other layers C_i with $i > 1$ or combinations thereof (data not shown). Activated SHP-1 associates with the TCR complex via Lck, triggering rapid dephosphorylation (19), but its precise mode of action is not quite clear yet (28). We simplify this whole process by assuming the dephosphorylation rate of each complex in the cascade increases linearly with S (activated SHP-1).

Downstream signaling of the previous phosphorylation cascade includes several positive feedbacks. Double-phosphorylated ITAMs eventually drive the phosphorylation of ERK, via binding and activation of zeta-chain-associated protein kinase 70 (ZAP70) and other kinases. Phosphorylated ERK is essentially bimodal in a cell population (20), and we use it as a proxy for T-cell activation. It acts indirectly by preventing SHP-1 from applying a brake on the cascade, and therefore amplifies the primary trigger. We choose to break up this process fully modeled in the studies by Altan-Bonnet and Germain (14) and Lipniacki et al. (20). As we shall see below, ERK phosphorylation does not add to our phenotypic model, and is therefore not considered. For the same reason, we do not include other known downstream positive regulations, such as bistability due to *Son of Sevenless* (*SOS*) signaling, which plays a role in digitalizing the response (27, 29). Instead, we simply assume that if the steady-state concentration of the last complex of the cascade, C_N, is higher than a threshold (which is a fixed parameter K of our model), response (and thus phosphorylated ERK) is turned on, similar to classical KPR. In other words, we coarse-grain binding of ZAP70 to double-phosphorylated ITAMs and subsequent stabilization and digitalization of response.

Details of our model, as well as mathematical derivations, are presented in *SI Appendix*. Interestingly, the steady state of the system is simple enough to be completely computed analytically, which considerably enhances our understanding, as detailed below. Variables in the model are the phosphorylated complexes C_i and the active form of the SHP-1 phosphatase (S). We add only four parameters relative to the KPR scheme to account for phosphatase influence and dynamics. At steady state, which is sufficient to understand most properties of the system, only two extra parameters matter, the typical concentration of phosphorylated complex to activate SHP-1 (which we call C_s) and the rescaled concentration of SHP-1 (γS_T).

Table 1 presents typical parameters we used. Following Altan-Bonnet and Germain (14), the numbers of receptors (R) and SHP-1 phosphatases (S_T) are assumed to be of the order of 30,000 and 600,000, respectively. The number of steps, N, in the cascade does not need to be large to see most of the effects described here ($N = 2$ is sufficient; see below); however, a larger N gives more parameter flexibility, and we take $N = 5$. Kinetic

Table 1. Summary of reference parameters used

Parameter name	Value	Description
R	30,000	Receptors per cell
κ	$10^{-4}\cdot s^{-1}$	Ligand/receptor association rate
ν	0.1–1 s^{-1}	Dissociation rate (inverse of dissociation time) for agonist and antagonist regimes
N	5	Number of phosphorylation steps
ϕ	0.09 s^{-1}	Phosphorylation rate
b	0.04 s^{-1}	Spontaneous dephosphorylation rate
K	0.2	Threshold for activation of response
C_S	500	Threshold for 50% activation of phosphatase
γ	$1.2 \times 10^{-6}\cdot s^{-1}$	Phosphatase efficiency
S_T	600,000	Phosphatase per cell

Numbers used are similar to those used by Altan-Bonnet and Germain (14). Note that there is no concentration unit: All parameters are expressed in actual molecules number per cell [e.g., $\kappa = 10^{-4}$ $(\text{molecule}\cdot s)^{-1}$].

parameters are unknown, but given that the order of magnitude of the discrimination threshold for dissociation time is ~3 s, it is consistent to assume that all relevant time scales of the system are roughly of this order, including the product κR maximum (de-)phosphorylation rates. We also make the conservative assumption that all ligands have comparable binding strength κ (as explained above, it is expected that ligands with much bigger κ would yield more response). A single ligand can trigger response (7); thus, our effective threshold for activation of K has to be lower than one molecule per cell, and we take it equal to 0.2 molecule per cell. From a practical standpoint, this means that the full real system must perform some noise smoothing/filtering, as we discuss in the section on the stochastic dynamics. The deterministic model is nevertheless informative, and we present it first because it is amenable to analytical solution, is more intuitive, and gives similar qualitative results. We expect kinetic parameters to vary quite significantly among immune cells because of their intrinsic variability. Indeed, we shall show that parameter variation yields variability in the behavior at the population level that our model can recover.

We first present in Fig. 1 the deterministic behavior of our model for varying concentrations of ligand L and a range of different dissociation times τ (Fig. 1*C*). The behavior is contrasted with pure KPR (Fig. 1*D*) to visualize better the crucial role of feedback effects. Numerical integration of the ordinary differential equations of the model (solid lines, Fig. 1*C*) is also compared with the analytical approximation computed in Eq. **S28** (crosses) in *SI Appendix*. The agreement is perfect for nonsaturating ligand concentrations.

For very low concentration of ligands L, the concentration C_N is linear in L with a slope depending on the dissociation time τ (*SI Appendix*). The behavior of the whole system is identical to classical KPR (Fig. 1 *C* and *D*) simply due to the number of ligands in Fig. 1*C* being too low to activate the SHP-1 negative feedback significantly. As the ligand concentration increases, SHP-1 gets activated (Fig. 1*E*). Steady-state concentration of SHP-1 activity is a Michaelis–Menten function of the first phosphorylated complex C_1 and roughly increases linearly with ligand concentration (Fig. 1*E*), before saturating. Increase of SHP-1 is the cause of the observed differences between our model and classical KPR (Fig. 1*D*). Specifically, SHP-1 acts qualitatively as a brake on C_N accumulation, resulting in overall flattening of the response over several orders of magnitude in L. Thus, for very strong antigens (high τ), C_N concentration first goes through a maximum before decreasing for ligands higher than 100 (Fig. 1*C*), although still remaining above threshold. Fig. 1 *C* and *D* make it clear that the nonmonotonic behavior of C_N is only due to the SHP-1 negative feedback, with no appreciable effect of receptor saturation (which happens at concentrations above tens of thousands). For the sake of our discussion, we can actually consider that receptors are never saturated (as confirmed by Fig. 1 *C* and *D*).

Our simple model explains both the sensitivity and specificity of early T-cell response. For instance, in Fig. 1*D*, we clearly see that the range of discrimination between antigens with $\tau = 10$ s (activated by 10 ligands) and $\tau = 3$ s (activated by 600 ligands) is less than two orders of magnitude for a KPR model. On the contrary, in Fig. 1*C*, the flattening of the curve at high ligand concentration due to the SHP-1 feedback activation maintains the concentration of C_N for $\tau = 3$ s below the threshold of activation K (chosen slightly higher than this "plateau" value). The consequence is that even a large number of ligands with $\tau = 3$ s will not elicit T-cell activation because of SHP-1 inhibition. Conversely, for $\tau = 10$ s, the system is in the KPR regime at low concentration and triggers an early response. Thus, our model is extremely sensitive to ligands with $\tau = 10$ s (or larger) and does not respond to ligands with $\tau = 3$ s (or smaller), almost irrespective of their concentration, as in the ideal scheme of Fig. 1*A*. Note that because C_N is necessarily smaller than the number of ligands presented, agonist detection at minute concentration constrains our threshold of activation K to be, at most, of the order of a few ligands per cell. We checked that parameters could be changed consistently to give similar qualitative behavior with values of K up to this limit (stochastic simulations are discussed below).

The response diagram τ vs. L for our model is summarized in Fig. 1*F*: Within half a decade of variation in τ, the minimum number of ligands required to activate falls from infinity to 10. Full dynamical simulations also show that the system quickly reaches equilibrium, in tens of seconds, consistent with the observed speed (*SI Appendix*, Fig. S1), the experimental data from Altan-Bonnet and Germain (14), and in figure 4*B* of ref. 21. We conclude that the simple addition of a negative feedback to KPR allows it to reproduce crucial properties of specificity, sensitivity, and response time of the early T-cell antigen discrimination process.

Digital vs. Analog Behavior as a Consequence of Decreasing Response at High Ligands. We have shown above that our model predicts a specific nonmonotonic behavior of the effector C_N, with a "bump" of maximum activity at intermediate ligand concentration, followed by a decrease and a final increase at very high concentration. This behavior is schematized in Fig. 2 by distinguishing three regimes of low, middle, and high ligand concentration that we analyze in more detail hereafter.

As explained earlier, at low ligand concentration per cell, the system behaves like a classical KPR scheme (blue slopes in Fig. 2*A*). The level of the last component of the phosphorylation cascade C_N is linear in ligand number, and the coefficient of proportionality is an increasing function of phosphorylation rate ϕ and binding time τ. At intermediate ligand concentration, the system turns on the

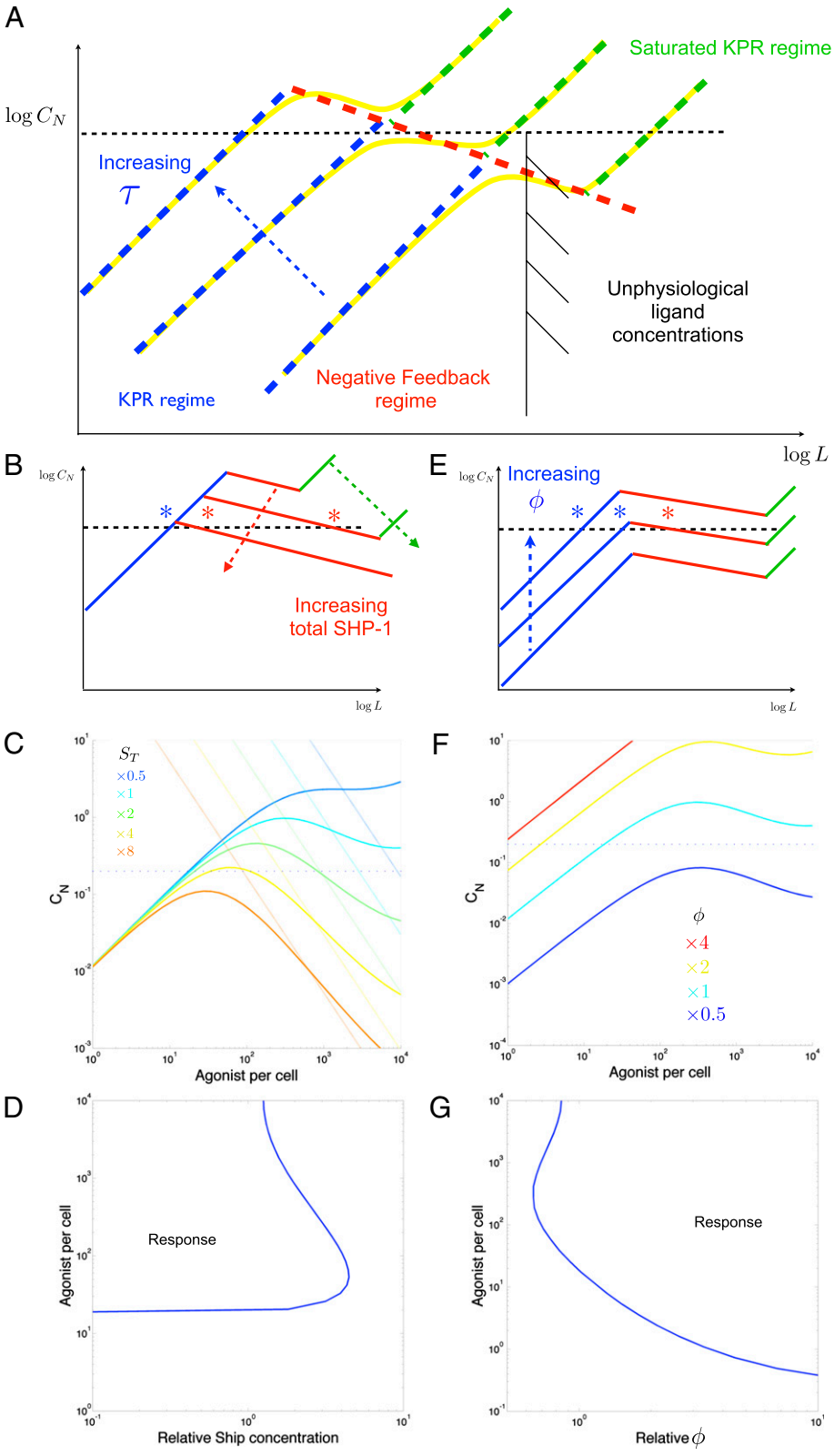

Fig. 2. Summary of parameter dependencies and digital/analog response for the deterministic system. (*A*, *B*, and *E*) Blue slope symbolizes the KPR regime of the response, the red slope symbolizes the negative feedback part of the response where phosphatase is activated, and the green slope symbolizes the saturated regime for the negative feedback. The dotted line indicates the threshold of activation of response by C_N . Blue stars indicate the position of first activation of response, and red stars indicate the position of deactivation of response. All simulations are for agonist dissociation time $\tau = 10$ s (*A*) Schematic of the three regimes at low, intermediate, and high antigen concentrations. The solid yellow lines indicate the interpolation for three different values of dissociation times. (*B*) Qualitative effect of phosphatase increase. The KPR part of the response (blue) is unchanged, whereas the negative feedback slopes move toward the left and the saturated regime on the right disappears. As the phosphatase increases, the response gets deactivated at higher concentration. (*C*) Numerical integration of the model with increasing SHP-1 concentration (solid lines; blue to orange indicate, respectively, γS_T = 50%, 100%, 200%, 400%, and 800% of reference value used for integrations of Fig. 1). The oblique dashed lines indicate the theoretical asymptotic slope for the negative feedback computed in *SI Appendix*, showing that the behavior gets closer to it as phosphatase increases. The dashed line is the threshold of activation. (*D*) Phase diagram computed numerically shows the antigen concentration triggering response as a function of relative SHP-1 concentration (with Fig. 1 being the reference). The response is abolished for a fourfold increase of SHP-1. (*E*) Qualitative effect of phosphorylation rate ϕ increase. Both the KPR part of the response and the negative feedback part of the response increase. (*F*) Numerical integration of the model with increasing ϕ (solid lines; blue to red indicate, respectively, ϕ= 50%, 100%, 200%, and 400% of reference value used for integrations of Fig. 1). (*G*) Phase diagram computed numerically shows the antigen concentration triggering response as a function of relative phosphorylation rate (with Fig. 1 being the reference). As phosphorylation rates increase, the minimum antigen concentration for activation decreases continuously.

negative feedback (Fig. 1*E*). In *SI Appendix*, we show mathematically that the net result of the competition between ligand increase and SHP-1 activation is the decrease of C_N. The magnitude of this decrease can be solved exactly with the help of the simplifying assumptions detailed in *SI Appendix* (Fig. S2 and Eq. **S48**), and the resulting scaling law is $C_N \propto \left(\frac{\phi C_S}{S_T}\right)^{N/2} L^{1-N/2}$. In a log-log plot, this gives a slope $1-\frac{N}{2}$ at high ligand concentration (red slope in Fig. 2*A*), which is a decreasing function of L if $N > 2$ (i.e., if the TCR–ligand complex can be phosphorylated more than twice). Interestingly, this asymptotic negative feedback regime is independent of the dissociation time (*SI Appendix*). Finally, at high ligand concentration, activation of the phosphatase

saturates and the system reaches a new KPR regime, with a maximum backward rate $b + \gamma S_T$, and therefore a downward shift in log-log plots with respect to the low ligand regime (green slope in Fig. 2*A*). This regime is actually barely attained in our simulations (for high dissociation times) and, given the typical number of receptors, is dampened by receptor saturation.

Summarizing the previous paragraphs, the full behavior of C_N essentially interpolates between three successive regimes (Fig. 2*A*). The position of the bump in C_N, corresponding to the maximum of the response, is expected to be roughly where the first two regimes [KPR regime (blue slope in Fig. 2) and the negative feedback regime (red slope in Fig. 2)] meet. Because the KPR regime is lifted up for ligands with high dissociation times, the negative feedback regime is met only for these ligands, explaining the flattening of the response curve. (More quantitatively, in *SI Appendix*, we show that all parameters being the same, the ligand concentration corresponding to the maximum response is inversely proportional to S_T, the phosphatase SHP-1 concentration).

An important consequence of the previous arguments relates to the effect of S_T. When we increase it, keeping all other parameters fixed, there are two effects: first, the fully activated regime for the phosphatase shifts toward very high ligand concentration, and therefore essentially disappears; second, because of the increase of available phosphatase, the negative feedback gets stronger and closer to its asymptotic behavior as computed above. As detailed earlier, C_N is a decreasing function of ligand concentration in the negative feedback regime. Therefore, in the high ligand region, where the effect of negative feedback is maximal, an increase of S_T can push the response below threshold, until response is totally abolished [red stars in Fig. 2*B* (moving from right to left) and Fig. 2*C*]. On the contrary, at low ligand concentration, the system remains in its KPR regime irrespective of phosphatase concentration, such that the minimum ligand concentration activating the response (blue star in Fig. 2*B*) is unchanged.

It follows that in a population of T cells with variable SHP-1 concentrations, we expect that cells trigger a response roughly for the same agonist concentration (with all of them being in the KPR regime), but response disappears at high ligand concentration for cells with high SHP-1 (Fig. 2 *B* and *C*). The combination of these two properties is a characteristic of our model and a direct consequence of the C_N decrease due to the negative feedback at high ligand concentration. Strikingly, this corresponds exactly to the digital effect observed experimentally in cells with increasing SHP-1 concentration (21): Agonist concentration for activation does not change, but the proportion of responding cells gradually decreases until response is abolished (stochastic simulations confirming this effect even in the presence of molecular noise are discussed below). Fig. 2*D* shows the ligand concentration triggering response for agonist $\tau = 10$ s with varying phosphatase concentrations. The low agonist boundary is flat (i.e., independent of SHP-1), whereas the response is very abruptly abolished above a threshold SHP-1 concentration.

The previous digital behavior was contrasted by Feinerman et al. (21) to the analog response when varying CD8 coreceptor concentration. CD8 recruits the kinase Lck; thus, it is natural to assume that the phosphorylation rate ϕ increases with CD8 in our model. Varying this parameter shifts up the whole response curve, modifying the position of the leftmost KPR slope (Fig. 2 *E* and *F*) and smoothly changing the agonist threshold for activation (blue star moving from right to left in Fig. 2*E*). Fig. 2*G* shows the ligand concentration triggering response for agonist $\tau = 10$ s continuously varying with ϕ in our model, confirming the analog effect observed by Feinerman et al. (21). Moreover, our model predicts that the immune response for weak agonists (close to the activation threshold) should disappear at high agonist concentration (red star in Fig. 2*E*). This effect, which is caused by the decrease of C_N due to the negative feedback, was indeed experimentally observed in figure 4 *B* and *C* of ref. 14, yet no explanation was provided (stochastic simulations confirming this effect are discussed below).

Antagonism. Previous sections have dealt with the response to a single type of ligand. We move now to mixtures of different antigens. It is indeed experimentally known that the response to agonists is inhibited (antagonized) when cells are exposed to a mixture of agonists and a high concentration of ligands with dissociation time below the threshold for activation (antagonists) (18). For instance, Altan-Bonnet and Germain (14) showed that the minimum amount of agonist needed to trigger response in the presence of 1–10 μM antagonists shifts from 1 to more than 1,000. A naive hypothesis is that antagonism is due to ligands competing for receptors. However, experiments show that antagonism is present even without cross-inhibition at the receptor level (18, 30) and that SHP-1 is an important effector of antagonism (19).

Let us proceed to a quantitative description of antagonistic effects in our model.

Two different ligands L_1(agonist) and L_2 (antagonist) with different binding times τ_1 and τ_2 are introduced. Both bind to (and possibly compete for) the same receptor R, forming multiply phosphorylated complexes denoted as C_i and D_i, respectively (details are provided in legend for Fig. 3 and *SI Appendix*). This description gives two sources of cross-talk between the ligands. The first is the sequestration and competition for the receptors. In agreement with experiments, we show below that this effect is negligible. The second, which turns out to be the source of antagonism, is that the phosphatase SHP-1 is activated in a symmetrical way by both C_1 and $D_1$and feeds back identically on both types of complexes, C_i and D_i. The activation of the downstream immune response is driven by the combined effect of both final complexes (i.e., $C_N + D_N$) (Fig. 3*A*).

In our model, if a cell is independently exposed to a few agonists L_1 (complexes C_i) or thousands of antagonists L_2 (complexes D_i), we clearly have, from Fig. 1*C*, $C_N \gg D_N$ because agonists trigger response, whereas antagonists do not. On the contrary, we have $C_1 \ll D_1$ or, similarly, from Fig. 1*E*, much more SHP-1 becomes activated for a cell exposed to thousands of antagonists than for a cell exposed to a few agonists. When a single cell is simultaneously exposed to few agonists and thousands of antagonists, coupling occurs via SHP-1, which is then essentially controlled by antagonists. From Fig. 3 (and analytical calculations in *SI Appendix*), it is then possible to grasp the basic mechanisms shaping antagonistic effects. The concentration of the activated phosphatase is higher for an antagonist with binding time $\tau_2 \simeq 3$ s than for $\tau_2 \simeq 1$ s. Because SHP-1 acts as a "brake" on phosphorylation, negative feedback is stronger for the former than for the latter (Fig. 3 *B* and *C*). This explains the striking observation reported by Altan-Bonnet and Germain (14) that antagonism gets stronger as the binding time of the antagonist increases (still remaining, of course, below the threshold of activation).

Using our phenotypic model, we predicted one additional quantitative effect for τ_2 closer to the agonist dissociation time. In the absence of agonist, the concentration of D_N (even though still smaller than the threshold of activation) is higher for $\tau_2 \simeq 3$ s than for $\tau_2 \simeq 1$ s at high antagonist L_2 concentrations (Fig. 3 *B* and *C*). Thus, the response curve for $\tau_2 \simeq 3$ s starts higher at low agonist levels but rises with L_1 less rapidly (because activated SHP-1 is higher) than the curve for $\tau_2 \simeq 1$ s. The winner of this race depends, in general, on the parameters of the dynamics and, most importantly, on the amount of antagonist present.

For small amounts of antagonists L_2 (Fig. 3*B*), the level of $C_N + D_N$ in the absence of agonist is far away from the threshold and is dominated by SHP-1 activity. This explains why ligands

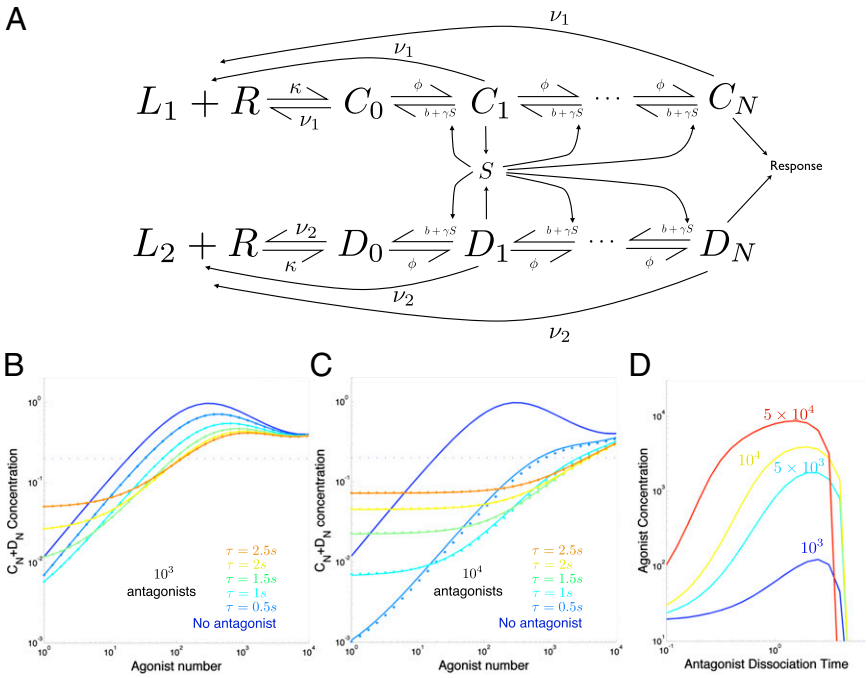

Fig. 3. Scheme of our model for the response to mixtures of antigens; antagonistic effects. (*A*) Schematic of the interactions with two types of ligands L_1 and L_2, with different dissociation times. Ligands are engaged in parallel at the same time in the same cell. Both activate the negative feedback symmetrically and contribute to the triggering of response. (*B*) Total response $C_N + D_N$ as a function of agonist concentration L_1 (τ=10s) in the presence of 10^3 antagonists $L_2$with dissociation times of 0.5, 1, 1.5, 2, and 2.5 s (light blue to orange). Dark blue indicates the response without any antagonist. Crosses indicate the analytical approximation detailed in *SI Appendix* showing perfect agreement. Other parameters are as in Fig. 1. (*C*) Same as *B*, but with $L_2 = 10^4$ antagonists, shows a strong dependency of antagonism on the antagonist concentration. (*D*) Agonist concentration L_1 triggering response as a function of antagonist concentrations L_2 and dissociation time. Dark blue, light blue, yellow, and red correspond to 1,000, 5,000, 10,000, and 50,000 L_2 ligands, respectively. As the quantity of antagonists increases, the maximum dissociation time for response decreases. It should be noted that the maximum concentration L_1 triggering response goes through a maximum shortly before its sharp collapse; this explains why antagonism is maximum for dissociation times just below the agonist regime.

with a longer dissociation time antagonize more than those with a shorter dissociation time. When the amount of antagonist is increased (Fig. 3*C*), the threshold is approached even in the absence of any agonist and even high SHP-1 activity can no longer prevent response if there are too many nonagonist ligands. This effect is illustrated in Fig. 3*D*. As the concentration of antagonists gets higher, the agonist level that elicits a response is no longer monotonously increasing with the binding time τ_2; this is also a prediction of our model that was unexplained by Altan-Bonnet and Germain (14). Thus, the relative strength of antagonists cannot be ranked simply by their binding time without reference to their concentration.

Stochastic Simulations and Experimental Comparison. In the previous sections, we have been working with deterministic differential equations and have set a threshold for activation, which is then digital, with a sharp transition from none to full response. Experimentally, the response is smoothed out at the population level. A number of reasons are potentially responsible for the smoothing, ranging from the diversity in the population to molecular noise effects in the dynamics (31). In fact, noise sensitivity motivated the proposal that dimerization between agonists and endogenous ligands was required to amplify response at concentrations of a few agonists per cell (22). The purpose of this section is twofold. First, we discuss the results of numerical simulations with the Gillespie algorithm (32). The Gillespie algorithm (32) is a computational method to simulate stochastic chemical systems and is needed when the number of molecules involved in the reactions is limited. Because these situations are rather frequent in biology, the algorithm has become the standard tool for the simulation of noisy biological systems. Here, we use the method to show that properties of our model are essentially unchanged when molecular noise is taken into account. Second, we present previous and new experimental data to compare predictions of our model with experiments.

When our model of receptor activation is made stochastic, the steady-state limit no longer applies and the fraction of responding cells depends on the time of observation, whose precise value is not very important provided it is several times larger than the relevant inverse rates in Table 1. It is plausible and we will explicitly show that the proximity of the deterministic C_N to the activation threshold K controls both the mean response time and the fraction of cells that respond in a given time. Thus, the stochastic model will round transitions but will not result in any new qualitative behavior.

Molecular noise is most relevant for species present in the smallest numbers (i.e., C_is, which are all bounded by the number of ligands, and C_N, which activates at a mean concentration K of the order of one per cell or less). The number of receptors upstream or the number of Zap70 kinases immediately downstream is much larger (30,000 or 10^6), and can be safely taken to be deterministic. The components downstream of Zap70 account for most of the complexity of the network in the studies by Altan-Bonnet and Germain (14), Lipniacki et al. (20), and Das et al. (27), and they both amplify and digitize (via ERK and SOS feedbacks) the signal. However, ligand discrimination is based on the signal from the receptors, and that is where our model terminates. Because the number of SHP-1 molecules is also very large, we assume a quasiequilibrium value of $S = S_T \frac{C_1(t)}{C_1(t)+C_S}$, where the parameter C_S is the typical concentration of phosphorylated complex to activate SHP-1. Our integration scheme is analogous to the one by Cao et al. (33). Further details of the stochastic simulations are reserved for *SI Appendix*.

To capture the essential effects and parameters, we assume then that the activation decision is based on imposing a threshold on the (running) average in time of the fully phosphorylated complexes (e.g., C_N; details are provided in *SI Appendix*). There is no shortage of modules that could be performing such a time integration in the multiple pathways downstream of Zap70. In our deterministic model, we set our activation threshold at $K = 0.2$ molecules of C_N per cell [this low value gives the best agreement with our stochastic simulations under the assumption that one single ligand can trigger response (7)]. We posit that C_N acts as an enzyme, phosphorylating Zap70; thus, it does not matter that this value is small as long as its activity gets integrated. Time integration is further needed to smooth out the huge level of fluctuations expected from such a small number of triggering ligands. With our current parameters, activation would indeed occur if at least one C_N molecule is present for 20 s. This value is compatible with the observed time scales and phenomenology.

We use our stochastic simulations to confirm, recapitulate, and extend experimental predictions of our deterministic model. Results of simulations computing the fraction of activated T cells vs. ligand level are shown in Fig. 4*A* for a set of ligand binding times that span the whole range from strong agonist to antagonist. We also show the average time of activation for activated cells in Fig. 4*B*. There is a good correspondence with the deterministic model in Fig. 1, namely, between the concentration for 50% activation in the stochastic model and the ligand concentration, such that C_N passes the deterministic threshold of activation. Note that no extra multimerization is necessary to explain the sensitivity and specificity of the system, contrary to the findings of Wylie et al. (22). Thus, even in the presence of noise, our model is still sensitive and specific (1).

The counterintuitive effect observed by Altan-Bonnet and Germain (14), that there is a decrease of the proportion of responding cells at high ligand concentrations for a weak agonist (in our parameters, $\tau_2 \simeq 5$ s), is confirmed even in the presence of noise (Fig. 4*A*). Our model also explains the nonmonotonic characteristic of average activation time observed in figures 3 *A* and *C* of ref. 14 but left unexplained, with a minimum for agonist concentrations around 400 (Fig. 4*B*). Again, these extrema for response to weak agonists and response time at middle range concentration reflect the maximum in C_N seen for similar ligand levels in Fig. 1, itself a consequence of the decreasing negative feedback regime detailed in Fig. 2.

Stochastic simulations for increased phosphatase concentration S_T are presented in Fig. 4*C*. The drop in the percentage of responding cells at high agonist concentration clearly corresponds to the shutting down of the response in the deterministic model (Fig. 2 *B* and *C*). Stochastic simulations for the activation curves at variable S_T levels are shown in Fig. 4*C*. Increasing S_T leaves the inflection point on the rising portion of the curves largely invariant, although greatly attenuating the response for agonist levels beyond the inflection. This explains what was termed the digital response to SHP-1 concentration by Feinerman et al. (21). The pronounced maximum, and then drop off, in response is a consequence of the existence of a maximum in the deterministic C_N curves as in Fig. 2, which just grazes the activation threshold for S_T larger than four times reference. This counterintuitive effect was actually seen in figure 2*B* of ref. 21, which we redraw in Fig. 4*D*. Calibration reveals that 10^{-2} μmol corresponds to roughly 3,000–10,000 ligands per cell (21); thus, the absolute position of the maximum response agrees well with theory.

Fig. 5*A* presents the simulation results for the proportion of responding cells in the presence of different antagonists, with corresponding new experiments in Fig. 5*B* confirming the behavior found in figures *D* and *E* of ref. 14. In our simulations, the minimum agonist concentration to trigger response shifts from 1 to more than 1,000 in the presence of strong antagonists is similar to what was found by Altan-Bonnet and Germain (14). This shift is more modest in our new data (Fig. 5*B*); the quantitative discrepancy between earlier and new data is attributed to the difference in SHP-1 concentration between experiments. Lower SHP-1 clearly yields less antagonism in our simulations, as shown in Fig. 5*C*.

The correspondence with Fig. 3 is clear: High concentration of strong antagonists (corresponding to $\tau_2 \simeq 2$ s) results in de-

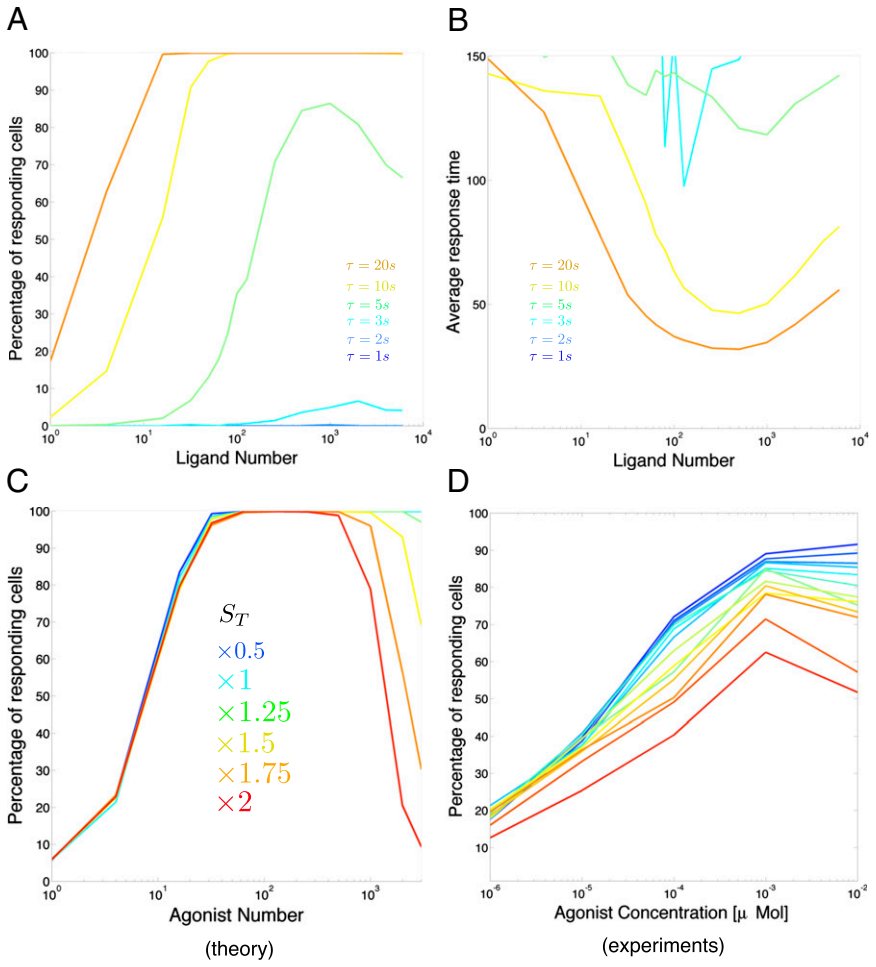

Fig. 4. Comparison between stochastic simulations, assuming quasistatic SHP-1 concentration, and experimental results. Parameters are as in Table 1. The percentage of active cells is computed over a total number of 1,000 realizations for each of the binding times and ligands. (*A*) Percentage of responding cells as a function of antigen number; different colors correspond to different dissociation times following the conventions of Fig. 1*B*. (*B*) Average response times (seconds) of responding cells for simulations of *A* show a minimum response time for ligands between 100 and 1,000 [as observed by Altan-Bonnet and Germain (14)]. (*C*) Percentage of responding cells as a function of increasing SHP-1 concentration. Conventions follow Fig. 2*C*. As SHP-1 increases, fewer and fewer cells are responding at high concentration. (*D*) Percentage of responding cells with increasing SHP-1 concentration, redrawn from the study by Feinerman et al. (21), shows collapse of response. In these experiments, total SHP-1 concentration varies from 0.1-fold (blue) to 2.5-fold reference (red). Calibration reveals that 10^{-2} μmol corresponds roughly to 3,000–10,000 ligands per cell (21). Thus, the agreement on the position of the decrease in response at high ligand concentration between simulations and experiments is very good. The strength of collapse is weaker than in *C*, which could be because of either a lower SHP-1 reference concentration or response smoothening due to other forms of noise (e.g., on parameters).

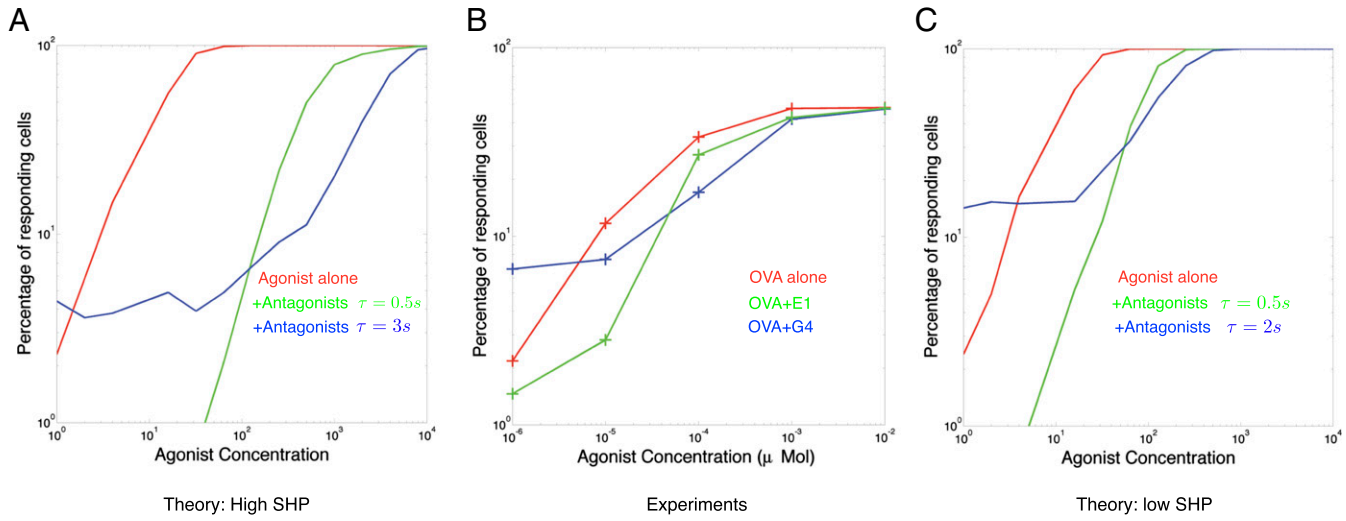

Fig. 5. Comparison between stochastic simulations and experimental results for antagonism. (*A*) Simulation of the percentage of responding cells for the standard parameters in Table 1 and an agonist with τ_1 = 10 s (red); then, the same agonist with 10,000 antagonistic ligands with τ_2 = 0.5 s (green) and τ_2 = 3 s (blue). We see the same trends as in Fig. 3, with more responding cells for the strong antagonist at low ligand concentration and the reverse relation at larger agonist levels. (*B*) Percentage of responding cells after 5 min as a function of ligand concentration for ovalbumin (OVA) ligands alone (red), OVA + 10 μmol of E1 ligands (green), and OVA +10 μmol of G4 ligands (blue). The trends are the same as in the simulation in *A*, and the fraction of cells responding when G4 is present follows the strong antagonist simulations. Antagonistic effects for these cells are less dramatic than in *A* and previously published data (notably ref. 14), suggestive of smaller SHP-1 concentration. (*C*) Stochastic simulation similar to *A* with half of the SHP-1 concentration in Table 1 and using a dissociation time of 2 s for strong antagonist gives better quantitative agreement with the experiments in *B*.

terministic levels C_N very close to the activation threshold even in the absence of the agonists. If we include stochastic effects, more cells are going to "leak" through the threshold and become activated even at low agonist concentration. Our full stochastic simulations confirm this effect: At low agonist concentration, 10% of cells exposed to 10^4 ligands with $\tau_2 \simeq 2$ s respond, whereas cells exposed to the same quantity of ligands with $\tau_2 \simeq 0.5$ s do not (Fig. 5 *A* and *C*). On the contrary, at intermediate ligand concentration, activity of the negative feedback dominates and is higher for ligands with $\tau_2 \simeq 2$ s. This explains the very characteristic crossing between curves in Fig. 5 *A* and *C*, which is checked experimentally in Fig. 5*B*: Blue curves (corresponding to longer τ_2) start higher than green curves at low ligand levels, but green curves increase much faster and get above blue curves at intermediate agonist levels. This is equivalent to saying that the stronger the antagonist, the higher is the fraction of responding cells at high antagonist concentrations, or that strong antagonists behave as weak agonists. This counterintuitive correlation is a characteristic of our model due to the fact that high concentration of ligands with dissociation times just below $\tau_2 \simeq 3$ s is close to activation threshold but, at the same time, maximally activates SHP-1 negative feedback (Figs. 1*E* and 3 *B* and *C*). As a consequence, there is a subtle balance due to the competition between the activity of ligands close to threshold and the negative feedback (Figs. 3*D* and 5), and antagonism is not an absolute property.

Discussion

We have proposed a simple analytical model for TCR antigen recognition, based on a KPR scheme modulated by a negative feedback loop. As detailed above, the model consistently recapitulates previous experimental observations (14, 21). Our phenotypic model predicts a crucial influence of the phosphatase SHP-1 controlling the negative feedback. In normal cells, activated SHP-1 controls the flattening of C_N for an intermediate range of ligands, which is necessary for sensitivity and specificity. If the concentration S_T of SHP-1 is too small, the efficiency of antigen discrimination is severely reduced and the response tends to become promiscuous at high antigen concentration. Conversely, if the concentration of SHP-1 S_T is too large, the strength of the negative feedback strongly increases with ligand concentration and we predict that the immune response then disappears for high agonist concentration, as confirmed experimentally in Fig. 4*D*, redrawn from the study by Feinerman et al. (21). Proper immune recognition therefore requires rather precise control of SHP-1 concentration. It is likely that this SHP-1 tuning is exploited in the immune system during thymic selection to control response as a function of the maturation stage and localization in the body of the T cells.

We analyzed antagonistic effects for mixtures of ligands and identified SHP-1 feedback as the key element in our model. We showed that decrease of SHP-1 results in less antagonism, as illustrated in our simulation and data in Fig. 5. Our model further predicts that the strength of antagonism is not an absolute property of the antagonist binding times but depends on the antagonist concentration as well.

Our model is deliberately both simple and conservative. The negative feedback integrates into a single effective linear term many elements, such as the interaction with Lck and the action of the phosphatase SHP-1. The final phosphorylations of ZAP-70 that trigger the response are conservatively modeled by a simple threshold, very similar to the original KPR (17). Experimental data that we analyzed are further downstream of the last phosphorylated complex C_N that we explicitly kept in our model. The ERK pathway and its positive feedback were, in fact, previously considered in great detail in the studies by Altan-Bonnet and Germain (14) and Lipniacki et al. (20), and it is known that they lead to discretization of the response via bistability (20). This was our rationale for truncating the network at the level of C_N and imposing a simple threshold of activation. Resulting simplifications have allowed us to reconsider and capture some puzzling qualitative effects left unexplained by Altan-Bonnet and Germain (14), such as the relation between the response time being minimum at intermediate ligand concentration and the nonmonotonic behavior of C_N, as illustrated in Fig. 4. Even when stochasticity is included, the model requires

neither amplification nor ligand heterodimerization to work, and we therefore refrained from including any.

Further experiments will be needed to quantify fully the total loss of response at the high agonist concentration that we predicted here for high S_T . The difficulty to overcome is the current lack of an appropriate SHP-1 antibody. It should also be possible to have direct experimental information on the phosphorylation state of the receptor complexes as a function of ligand concentration [via ZAP70 or linker for activation of T cells (LAT)]. No data are available at the current time, however, because they require a very good antibody to resolve the low concentrations at the threshold of activation.

Biological networks are manifestly very complicated. Our analysis provides a clear example of the interest of phenotypic models, simple enough to be studied mathematically but not oversimplified to the point of losing contact with experimental data. Covariation of levels of pathway components (e.g., via transcriptional coregulation and thymic selection) (21) certainly complicates the analysis for primary cells, but we predict that the main behavior can be understood via corresponding covariation of a small number of parameters. Then, we can connect these parameters to actual effectors of the system: phosphorylation rate ϕ to CD8 or Lck concentration and strength of the negative feedback S to SHP-1 concentration. Our model can, of course, be further refined; for example, it is possible that heterodimerization indeed contributes to amplification (23), but our study demonstrates that it is not required a priori, even in simple models with few components. It has also been shown very recently that only a few components (Lck, ZAP70, and CD45) are sufficient to recreate receptor triggering artificially without the need of receptor dimerization (34). This confirms the relevance of simple models with a small number of variables but leaves open the question of whether performance for sensitivity and specificity of synthetic systems matches natural ones.

Our approach is rather general and could potentially be applied to other phosphorylation cascades widespread in signaling pathways. We expect that some of the counterintuitive properties of the feedback by phosphatases that we exhibited and explained here should be shared with other signaling systems, opening the way to their unified theoretical description.

Experimental Procedures

Primary Cells. Splenocytes and lymphocytes were isolated from C57BL/6N mice (Taconic Farms) or OT-1 TCR transgenic mice (National Institute of Allergy and Infectious Diseases contract colony; Taconic Farms) on a recombination activating gene (RAG2)$^{-/-}$ C57BL/6N background and used to prepare cultures of primary cells. All mice were bred and maintained in accordance with the protocol (MSKCC 05-12-031) approved by the Institutional Animal Care and Use Committee of Memorial Sloan–Kettering Cancer Center.

Cell Line. RMA-S cells [transporter for antigen presentation (TAP)$^{-/-}$ T-cell lymphoma expressing H-2K^{b}] were used as APCs.

Antigen Peptides. The agonist ovalbumin peptide SIINFEKL (OVA) and its variants EIINFEKL (E1), SIIGFEKL (G4), SIITFEKL (T4), and SIIQFEKL (Q4) were obtained from Genscript.

Antibodies and other reagents are described in *SI Appendix, Supplementary Experimental Procedures*.

OT-1 T-cell cultures were used for the experiments. Their preparation, stimulation, and activation, as well as the antibody staining, are detailed in *SI Appendix, Supplementary Experimental Procedures*.

ACKNOWLEDGMENTS. Support for this work was provided by the Natural Science and Engineering Research Council of Canada Grant RGPIN 401950-11 and McGill University (P.F.); National Science Foundation Grant PHY-0954398 (to E.D.S.); National Science Foundation Grant MCB-0848030 and National Institutes of Health Grant AI083408 (to G.A.-B.); and the Fondation de France, Prix Lebrasseur (to M.V.).

1. Feinerman O, Germain RN, Altan-Bonnet G (2008) Quantitative challenges in understanding ligand discrimination by alphabeta T cells. *Mol Immunol* 45(3): 619–631.
2. Bousso P, Bhakta NR, Lewis RS, Robey E (2002) Dynamics of thymocyte-stromal cell interactions visualized by two-photon microscopy. *Science* 296(5574):1876–1880.
3. Bousso P, Robey E (2003) Dynamics of CD8+ T cell priming by dendritic cells in intact lymph nodes. *Nat Immunol* 4(6):579–585.
4. Bousso P, Robey EA (2004) Dynamic behavior of T cells and thymocytes in lymphoid organs as revealed by two-photon microscopy. *Immunity* 21(3):349–355.
5. Grakoui A, et al. (1999) The immunological synapse: A molecular machine controlling T cell activation. *Science* 285(5425):221–227.
6. Sykulev Y, Joo M, Vturina I, Tsomides TJ, Eisen HN (1996) Evidence that a single peptide-MHC complex on a target cell can elicit a cytolytic T cell response. *Immunity* 4(6):565–571.
7. Irvine DJ, Purbhoo MA, Krogsgaard M, Davis MM (2002) Direct observation of ligand recognition by T cells. *Nature* 419(6909):845–849.
8. Rojo JM, Janeway CA, Jr. (1988) The biologic activity of anti-T cell receptor V region monoclonal antibodies is determined by the epitope recognized. *J Immunol* 140(4): 1081–1088.
9. Gascoigne NR, Zal T, Alam SM (2001) T-cell receptor binding kinetics in T-cell development and activation. *Expert Rev Mol Med* 2001:1–17.
10. Govern CC, Paczosa MK, Chakraborty AK, Huseby ES (2010) Fast on-rates allow short dwell time ligands to activate T cells. *Proc Natl Acad Sci USA* 107(19):8724–8729.
11. Aleksic M, et al. (2010) Dependence of T cell antigen recognition on T cell receptor-peptide MHC confinement time. *Immunity* 32(2):163–174.
12. Huppa JB, et al. (2010) TCR-peptide-MHC interactions in situ show accelerated kinetics and increased affinity. *Nature* 463(7283):963–967.
13. Huang J, et al. (2010) The kinetics of two-dimensional TCR and pMHC interactions determine T-cell responsiveness. *Nature* 464(7290):932–936.
14. Altan-Bonnet G, Germain RN (2005) Modeling T cell antigen discrimination based on feedback control of digital ERK responses. *PLoS Biol* 3(11):e356.
15. Hopfield JJ (1974) Kinetic proofreading: A new mechanism for reducing errors in biosynthetic processes requiring high specificity. *Proc Natl Acad Sci USA* 71(10): 4135–4139.
16. Ninio J (1975) Kinetic amplification of enzyme discrimination. *Biochimie* 57(5): 587–595.
17. McKeithan TW (1995) Kinetic proofreading in T-cell receptor signal transduction. *Proc Natl Acad Sci USA* 92(11):5042–5046.
18. Dittel BN, Stefanova I, Germain RN, Janeway CA, Jr. (1999) Cross-antagonism of a T cell clone expressing two distinct T cell receptors. *Immunity* 11(3):289–298.
19. Stefanová I, et al. (2003) TCR ligand discrimination is enforced by competing ERK positive and SHP-1 negative feedback pathways. *Nat Immunol* 4(3):248–254.
20. Lipniacki T, Hat B, Faeder JR, Hlavacek WS (2008) Stochastic effects and bistability in T cell receptor signaling. *J Theor Biol* 254(1):110–122.
21. Feinerman O, Veiga J, Dorfman JR, Germain RN, Altan-Bonnet G (2008) Variability and robustness in T cell activation from regulated heterogeneity in protein levels. *Science* 321(5892):1081–1084.
22. Wylie DC, Das J, Chakraborty AK (2007) Sensitivity of T cells to antigen and antagonism emerges from differential regulation of the same molecular signaling module. *Proc Natl Acad Sci USA* 104(13):5533–5538.
23. Krogsgaard M, et al. (2005) Agonist/endogenous peptide-MHC heterodimers drive T cell activation and sensitivity. *Nature* 434(7030):238–243.
24. Yachi PP, Lotz C, Ampudia J, Gascoigne NR (2007) T cell activation enhancement by endogenous pMHC acts for both weak and strong agonists but varies with differentiation state. *J Exp Med* 204(11):2747–2757.
25. Ma Z, Sharp KA, Janmey PA, Finkel TH (2008) Surface-anchored monomeric agonist pMHCs alone trigger TCR with high sensitivity. *PLoS Biol* 6(2):e43.
26. Kersh EN, Shaw AS, Allen PM (1998) Fidelity of T cell activation through multistep T cell receptor zeta phosphorylation. *Science* 281(5376):572–575.
27. Das J, et al. (2009) Digital signaling and hysteresis characterize ras activation in lymphoid cells. *Cell* 136(2):337–351.
28. Neel BG, Gu H, Pao L (2003) The 'Shp'ing news: SH2 domain-containing tyrosine phosphatases in cell signaling. *Trends Biochem Sci* 28(6):284–293.
29. Prasad A, et al. (2009) Origin of the sharp boundary that discriminates positive and negative selection of thymocytes. *Proc Natl Acad Sci USA* 106(2):528–533.
30. Robertson JM, Evavold BD (1999) Cutting edge: dueling TCRs: Peptide antagonism of CD4+ T cells with dual antigen specificities. *J Immunol* 163(4):1750–1754.
31. Artyomov MN, Das J, Kardar M, Chakraborty AK (2007) Purely stochastic binary decisions in cell signaling models without underlying deterministic bistabilities. *Proc Natl Acad Sci USA* 104(48):18958–18963.
32. Gillespie DT (1977) Exact stochastic simulation of coupled chemical reactions. *J Phys Chem* 81(25):2340–2361.
33. Cao Y, Gillespie DT, Petzold LR (2005) The slow-scale stochastic simulation algorithm. *J Chem Phys* 122(1):14116.
34. James JR, Vale RD (2012) Biophysical mechanism of T-cell receptor triggering in a reconstituted system. *Nature* 487(7405):64–69.